

# “Self-trapping” in Solar Cell Hybrid Inorganic-Organic Perovskite Absorbers

Christian Tantardini\*,<sup>1,2</sup> Sebastian Kokott,<sup>3</sup> Xavier Gonze,<sup>2,4</sup> Sergey V. Levchenko\*,<sup>2</sup> and Wissam A. Saidi\*<sup>5</sup>

<sup>1</sup>*Institute of Solid State Chemistry and Mechanochemistry SB RAS, 630128 Novosibirsk, Russian Federation.*

<sup>2</sup>*Skolkovo Institute of Science and Technology, Skolkovo Innovation Center, Bolshoy boulevard 30, Moscow, 143026, Russian Federation.*

<sup>3</sup>*NOMAD Laboratory, Fritz-Haber-Institut der MPG, Faradayweg 4-6, 14195 Berlin, Germany.*

<sup>4</sup>*European Theoretical Spectroscopy Facility, Institute of Condensed Matter and Nanosciences, Université catholique de Louvain, Chemin des étoiles 8, bte L07.03.01, B-1348 Louvain-la-Neuve, Belgium*

<sup>5</sup>*Department of Mechanical Engineering and Materials Science, University of Pittsburgh, Pittsburgh, Pennsylvania 15261, United States.*

(Dated: January 5, 2023)

In the simplest picture, a “self-trapped” polaron forms when an excess electron or hole deforms a crystal lattice, creating a potential well with bound states. Properties of self-trapped polarons in methylammonium lead iodide perovskite (MAPbI<sub>3</sub>), which is widely used as solar cell absorber, are of great interest, and are a subject of ongoing investigations and debates concerning the existence of large polarons with the co-presence of metastable self-trapping. Herein, we employ a self-interaction-free density functional theory method to investigate the stability of small polarons in tetragonal MAPbI<sub>3</sub> phase. The electron small polaron is found to be unstable, while the hole small polaron is found to be metastable at realistic operation temperatures of solar cells. Further, the hole polaron is found to have a hole band close to the conduction band, which in conjunction with its metastability suggests that small polarons will have an appreciable effect on charge-carrier recombinations in MAPbI<sub>3</sub>. Further, we posit that the existence of the metastable polarons in addition to the large polarons may explain the experimentally observed non-monotonic temperature dependence of bimolecular charge-carrier recombination rate in tetragonal MAPbI<sub>3</sub> phase.

PACS numbers: To be checked : 71.20.Ps, 78.20.-e, 42.70.-a

## I. INTRODUCTION

The search for energy sources with less adversarial environmental impact is presently of fundamental importance for basic and applied scientific research. Metal-halide perovskite semiconductors have shown excellent performance in optoelectronic applications such as solar cells, light-emitting diodes, and detectors<sup>1–17</sup>. In particular, methylammonium lead iodide perovskite (MAPbI<sub>3</sub>) in its tetragonal phase, which is thermodynamically stable from 160 K to 315 K, is a promising solar absorber material, because it combines high power conversion efficiency and low cost, two key properties of a disruptive solar cell technology, which can secure long-term economic growth and would help to reduce the burning of fossil fuels to generate electrical energy. The race for power conversion efficiency is interdisciplinary, touching chemistry and physics at the same time, in addition being a very timely topic. Indeed, the class of metal-halide perovskites has achieved a solar power conversion efficiency equal to 22.1%, which is an impressive record considering that the first perovskite-based solar cell was fabricated only ten years ago<sup>2,9</sup>. In MAPbI<sub>3</sub> as in all infra-red active semiconductors, bare charge carriers are expected to dress and form polarons due to electron-phonon coupling arising e.g. from Fröhlich interaction with the longitudinal optical (LO) phonons<sup>18–20</sup>. A self-trapped polaron forms when an excess electron or hole deforms a crystal lattice creating a potential well with bound states. The extent of a polaron depends of the subunits where

it is localized. We define small polaron when polaron wavefunction is localized within the size of the order of the shortest inter-atomic distance. A large polaron is defined when the polaron wavefunction is delocalized on several unit cells. It is noteworthy that for photovoltaic applications, large polarons appear not to be significantly detrimental, while small polarons limit charge-carrier mobilities substantially and lead to charge-carrier self-trapping and fast non-radiative recombination<sup>19–23</sup>. Further, small polarons with an associated exciton can generate broadband luminescence, which is important for solid-state lighting as well as other applications such as gamma-ray detection<sup>24,25</sup>.

There is a large consensus in the metal-halide perovskite field that tetragonal MAPbI<sub>3</sub> phase is characterized by (i) a remarkable long-range diffusion length,  $L_D$ <sup>14,26–29</sup>; (ii) electron-hole recombination rates that are five orders of magnitude lower than that predicted by Langevin model<sup>14,17,20,30</sup>; (iii) temperature dependence of carrier mobility that follows  $\mu \propto T^{-(3/2)}$ <sup>29,31–38</sup>. In relation to (ii) one should however realize that the Langevin model generally applies to low-mobility semiconductors, and hence it is questionable whether it is applicable in the halide perovskites that have moderate carrier mobilities<sup>15</sup>.

Many experimental studies focused on charge-recombination in MAPbI<sub>3</sub> to explain the charge-carrier mobility<sup>14,15,17,31,39,40</sup>. The rates for charge-recombination can be correlated through a differential equation that describes the variation of charge carrier

density,  $n$ , as a function of pulsed excitation time,  $t$ :

$$\frac{\partial n}{\partial t} = G - k_1 n - k_2 n^2 - k_3 n^3 = G - n R_T(n), \quad (1)$$

where  $G$  is the charge-density generation rate,  $k_1$  is the monomolecular charge-recombination rate constant,  $k_2$  is the bimolecular electron-hole recombination rate constant, and  $k_3$  is the Auger recombination rate constant.  $R_T(n)$  is the total charge recombination rate, equal to  $k_1 + k_2 n + k_3 n^2$ .  $k_1$  describes by definition processes involving one ‘‘particle’’ at a time, which in a typical semiconductor may consist of a hole in the valence band, or an electron in the conduction band, or a combined electron-hole pair as an exciton.  $k_2$  describes the charge carrier recombination between electrons and holes in a direct semiconductor and can be viewed as the reverse process of light absorption by continuum states<sup>41</sup>.  $k_3$  describes a many-body process involving recombination of an electron with a hole, accompanied by energy and momentum transfer to a further electron or a hole, like in an Auger process. While Auger recombination is insignificant for the operation of photovoltaic cells at standard solar illumination intensities, it is likely to play a crucial role for the development of lasers based on metal-halide perovskites.<sup>42,43</sup>

In the most interesting tetragonal phase of MAPbI<sub>3</sub>,  $k_1$  monotonically is found to increase with temperature while  $k_2$  decreases non-monotonically with temperature and is associated with a small peak around room temperature<sup>14,15,17,31,39,40</sup>. The  $k_1$  temperature dependence is consistent with a charge recombination process assisted by ionized impurities. On the other hand, the decrease of  $k_2$  upon heating is consistent with the recombination between electrons in the conduction band and holes in the valence band, i.e., with large polarons. However, this interpretation does not explain the non-monotonic behaviour, as we elaborate below. In the large polaron regime, an early study included the effects coming from acoustic phonon scattering and described the carrier lifetime by the semi-classical Boltzmann transport theory<sup>44</sup>. However a later study more correctly took into account the polar-optical phonon mode scattering, leading to a mobility  $\mu$  proportional to  $T^{-(0.46)}$ <sup>20</sup>. This model however disagrees with optical-pump, terahertz-probe spectroscopy and time-resolved microwave conductivity (TRMC) measurements that although confirms a large polaron regime in tetragonal MAPbI<sub>3</sub> phase, shows  $\mu \propto T^{-(3/2)}$ <sup>14,15,17,31,39,40</sup>. The rapid decrease of the conductivity with temperature and the non-monotonic behavior of  $k_2$  are puzzling, and are particularly inconsistent with a picture where exclusively large polarons are charge carriers in tetragonal MAPbI<sub>3</sub> phase. While the temperature dependence of conductivity is influenced by several factors,  $k_2$  temperature dependence in these materials is determined only by the properties of polarons (small versus large). Thus, analysis of the variation of  $k_2$  with temperature allows us to understand the type

of charge carrier present. Namely, a monotonic decrease of  $k_2$  with increasing temperature is a signature of large polarons, while  $k_2$  should monotonically increase if self-trapping and small polaron formation occur. Therefore, the observed non-monotonic behavior of  $k_2$  in tetragonal MAPbI<sub>3</sub> phase around room temperature suggests the co-presence of small and large polarons. Moreover, the observed small Stokes shifts of the order of  $meV$  between absorption onset and photoluminescence emission peaks<sup>40,45</sup> also indicate a metastable small electron and/or hole polaron with an energy level close to valence band maximum and/or conduction band minimum, respectively.

Experimental results are supportive of the presence of metastable self-trapping in tetragonal MAPbI<sub>3</sub>, which is not seen in theoretical studies that show instead very stable self-trapping with stabilization energy on the order of  $eV$ <sup>46–48</sup>, or very unstable self-trapping with similar order of magnitude<sup>49</sup>. The disagreement between the theoretical studies as well as between experiment and theory reflects the inherent complexity of the first-principles description of polarons in semiconductors. The major problem is due to errors in standard exchange-correlation functional approximations of density-functional theory (DFT), in particular the self-interaction error (SIE). The  $GW$  approximation is a more accurate but computationally expensive approach to calculate electronic structure, which was successfully used to produce accurate calculations of the electronic band structure in agreement with experiments<sup>22,23,41,50–52</sup>. However, the computation of total energies within  $GW$  is challenging, and, consequently,  $GW$  has not been used to obtain the atomic structure of small polarons. Other studies focused on first-principles calculations of electron-phonon coupling<sup>44,52–54</sup>, without discussing the small polaron stability. Conventional local and semi-local exchange-correlation approximations in DFT, namely the local density approximation (LDA) and generalized gradient approximation (GGA), have been reported to lead to delocalization of the polaron over many unit cells due to SIE, which would lead to a severe overestimation of the polaron size<sup>55–58</sup>. DFT+ $U$  that typically works well for strongly correlated systems can be used to localize the polaronic states, but the results would strongly depend on the value of  $U$  that could require nonphysical values to localize the polaron state<sup>55–59</sup>. Furthermore, hybrid functionals depend on adjustable parameters, which are intrinsically affected by systems on which they were parameterised<sup>55–58</sup>. Thus, to correctly describe polaron self-trapping in MAPbI<sub>3</sub>, it is imperative to employ an approach that mitigates the SIE. Such an approach was introduced recently and was called *polaron* self-interaction correction (pSIC)<sup>55–58</sup>. In this work we will investigate electron and hole self-trapping in tetragonal MAPbI<sub>3</sub> using pSIC in conjunction with a method to also mitigate the artificial finite-size effects.<sup>55</sup> Given the importance of polarons in MAPbI<sub>3</sub>, we expect that our findings will have a strong impact on subsequent stud-

ies that are focused on efficiency improvements of solar absorbers with important scientific and economical consequences in this field.

Sections II and III present the development of polaron self-interaction correction theory and computational parameters, respectively. Our results are presented in Sec. IV, focusing first on polaron formation energies and associated atomic displacements, then analysing the electronic structure.

## II. THEORETICAL BACKGROUND

The binding energy of the hole  $E_{bind}^+$  or electron  $E_{bind}^-$  polaron can be computed as follows:

$$E_{bind}^{\pm} = E_{dist}(N_e \mp 1) - E_{perf}(N_e \mp 1), \quad (2)$$

where  $E_{dist}$  and  $E_{perf}$  are the total energies of the distorted and pristine structures, and the numbers in the parenthesis indicate the total number of electrons in the system, with  $N_e$  corresponding to the neutral case. A negative  $E_{bind}^{\pm}$  indicates an energy gain due to the distortion that results in self-trapping. In the Fröhlich model, in which the polaron is large compared to the unit cell, the long-range interaction of electrons or holes with polar phonon modes is always attractive and results in self-trapping for any polar crystal. In this model, by construction, there is no self-interaction of the electron or hole. For intermediate and strong electron-phonon coupling, short-range interactions become increasingly important as the polaron radius becomes comparable to the unit cell size. In such a case, the polaron formation cannot anymore be described by macroscopically averaged properties as in Fröhlich model, and a first-principles treatment at the atomic scale is needed.

The polaron as a special kind of point defect can be simulated from first-principles using a cluster or supercell approach by computing  $E_{bind}^{\pm}$  according to Eq. (2) with explicit charge. The cluster approach, if used without embedding, may lead to artificial localization and spurious boundary effects. On the other hand, the application of the standard supercell approach is challenging. First, the explicit use of charge leads to wrong long-range behavior due to the interaction with neighboring cells, which ought to be corrected *a posteriori* using Makov-Payne<sup>60</sup> or Freysoldt *et al.*<sup>61</sup> approaches. More importantly, typically charge localization in the pristine crystal takes place only if the supercell is chosen sufficiently large and self-interaction is reduced even in the case of strong electron-phonon coupling. (Semi-)local exchange-correlation functionals do not address the self-interaction problem, while hybrid functionals allow one to attenuate it by including some fraction of exact exchange, which is however an *ad hoc* procedure, and the results may be very sensitive to the fraction value.<sup>55</sup> All of this makes the supercell approach with explicit charges prone to large errors in MAPbI<sub>3</sub>, considering the weak to medium electron-phonon interactions.

Herein we use pSIC<sup>57,58</sup> in conjunction with Perdew-Burke-Ernzerhof (PBE)<sup>62</sup> and Heyd-Scuseria-Ernzerhof (HSE06) functionals.<sup>63</sup> Additionally, we account for van der Waals dispersion interactions using Tkatchenko-Scheffler (vdW-TS) method<sup>64</sup>, and spin-orbit coupling (SOC) effects using a perturbative approach<sup>65</sup>. In the following, we denote these approaches as PBE/HSE+SOC(vdW-TS). Our results as well as previous studies<sup>66-68</sup> show in particular that dispersion corrections are needed to accurately describe MAPbI<sub>3</sub>.

pSIC follows the supercell approach but computes the polaron structure and energetics by adding to the neutral system a small fractional charge and removing the quadratic dependence on this charge to predict the fully charged system, thus suppressing the interaction of this charge with itself. We briefly review the formalism. For the case of the hole polaron, the ionization energy (IP), which is the difference of total energies between systems with  $N_e - 1$  and  $N_e$  electrons, is connected with the highest occupied orbital for the neutral system  $\epsilon^{HOMO}(N_e)$ :

$$IP = E(N_e - 1) - E(N_e) = -\epsilon^{HOMO}(N_e). \quad (3)$$

Hence,  $E_{bind}^+$  from Eq. (2) becomes

$$E_{bind}^+ = \Delta E - \Delta\epsilon^{HOMO}, \quad (4)$$

where  $\Delta E = E_{dist}(N_e) - E_{perf}(N_e)$  and  $\Delta\epsilon^{HOMO} = \epsilon_{dist}^{HOMO}(N_e) - \epsilon_{perf}^{HOMO}(N_e)$ , both of which are evaluated for the neutral system.

In pSIC,<sup>57,58</sup>  $\epsilon^{HOMO}(N_e)$  is evaluated from Janak's theorem<sup>69</sup> and utilizes a finite-difference approximation of the derivative of the total energy under three different charge constraints, namely,

$$\begin{aligned} \epsilon^{HOMO}(N_e) &= \left. \frac{\partial E_{DFT}}{\partial N_e} \right|_{N_e - \delta} \\ &\approx \frac{1}{2\delta} \left( 3E_{DFT}[N_e] - 4E_{DFT}[N_e - \delta] \right. \\ &\quad \left. + E_{DFT}[N_e - 2\delta] \right), \end{aligned} \quad (5)$$

which eliminates the quadratic self-interaction within DFT, unlike the straight DFT evaluation of the IP in Eq.(3). In the second member of the equality Eq.(5),  $\delta$  is a positive infinitesimal. The optimized geometries are obtained by calculating the forces from the shifted potential energy surface  $E - \epsilon^{HOMO}$  of the neutral system derived from:

$$F_i^+ = -\nabla_i E + \nabla_i \epsilon^{HOMO} = -\nabla_i E_{pSIC}^+, \quad (6)$$

where  $i$  denotes a virtual displacement of some atom along a given direction. The first term in Eq. (6) is the usual force in the neutral system that is readily available from DFT calculations. The second term is the contribution from the highest occupied orbital, which is then approximated using the pSIC.

The pSIC formalism for the electron polaron is similar, starting with

$$EA = E(N_e + 1) - E(N_e) = +\epsilon^{LUMO}(N_e), \quad (7)$$

which connects the electronic affinity (EA) with the lowest unoccupied orbital for the neutral system  $\epsilon^{LUMO}(N_e)$ . In this case the  $E_{bind}^-$  of Eq. (2) becomes

$$E_{bind}^- = \Delta E + \Delta\epsilon^{LUMO}, \quad (8)$$

where  $\Delta E = E_{dist}(N_e) - E_{perf}(N_e)$  and  $\Delta\epsilon^{LUMO} = \epsilon_{dist}^{LUMO}(N_e) - \epsilon_{perf}^{LUMO}(N_e)$ , both of which are evaluated for the neutral system. In pSIC,  $\epsilon^{LUMO}(N_e)$  becomes

$$\begin{aligned} \epsilon^{LUMO}(N_e) &= \left. \frac{\partial E_{DFT}}{\partial N_e} \right|_{N_e + \delta} \\ &\approx \frac{1}{2\delta} \left( -3E_{DFT}[N_e] + 4E_{DFT}[N_e - \delta] \right. \\ &\quad \left. - E_{DFT}[N_e - 2\delta] \right). \end{aligned} \quad (9)$$

The optimized geometries are obtained by calculating the forces from the shifted potential-energy surface  $E + \epsilon^{LUMO}$  of the neutral system derived from:

$$F_i^- = -\nabla_i E - \nabla_i \epsilon^{LUMO}. \quad (10)$$

The distorted structures for hole and electron polarons are obtained by minimizing the pSIC forces computed from the DFT forces of the system under three different charge constraints, with the following explicit formula

$$\begin{aligned} \frac{\partial E_{pSIC}^\pm}{\partial \vec{R}_i} &= \left( 1 - \frac{3}{2\delta} \right) \frac{\partial E_{DFT}}{\partial \vec{R}_i} [N_e] \\ &+ \frac{1}{2\delta} \left( 4 \frac{\partial E_{DFT}}{\partial \vec{R}_i} [N_e \pm \delta] - \frac{\partial E_{DFT}}{\partial \vec{R}_i} [N_e \pm 2\delta] \right) \end{aligned} \quad (11)$$

Instead of the traditional approach that obtains the equilibrium configuration under  $\pm 1$  extra charge for the hole/electron polaron, this approach uses the forces from the neutral system and two additional calculations with small fractional charges  $\pm\delta$  and  $\pm 2\delta$ .  $E_{DFT}[N_e]$ ,  $E_{DFT}[N_e \pm \delta]$ , and  $E_{DFT}[N_e \pm 2\delta]$  are the energies of neutral and charged systems, and  $\frac{\partial E}{\partial \vec{R}_i}$  is the negative of the atomic force on atom  $i$  for each system. The variation of charge is generated by removing (hole) or adding (electron) electrons by a small amount  $\delta$ . With this approach, the remaining error due to numerical differentiation is  $O(\delta^3)$ . Thus,<sup>58</sup>

$$\begin{aligned} F_i^\pm &= F_i(N_e) \\ &+ \frac{1}{2\delta} \left[ 4F_i(N_e \mp \delta) - 3F_i(N_e) - F_i(N_e \mp 2\delta) \right] \end{aligned} \quad (12)$$

To optimize the structure, we use pSIC on top of PBE, which is believed to accurately predict band edge variations induced by geometry changes, if not the band gap itself.<sup>57,58,70,71</sup>

Sadigh *et al.*<sup>57,58,71</sup> showed that treating the polaron on the potential-energy surface for  $E_{bind}^\pm$  drastically reduces the impact of the underlying functional and, even with semi-local functionals like PBE, self-trapping of the polaron happens and can be relatively well described. However, Kokott *et al.*<sup>55</sup> showed that this approach leads to a strong dependence on the supercell size due to the long-range effects of ionic response, which can nevertheless be properly accounted for using a correction scheme<sup>55</sup>. The value for fractional charge  $\delta=0.025e$  was used in our calculations, in line with previous studies<sup>55</sup>.

### III. COMPUTATIONAL DETAILS

The DFT calculations are carried out using all-electron FHI-aims employing a tier-2 basis set for structural optimization and a tight tier-2 basis set to compute the energies and band structure. For the bulk tetragonal phase of MAPbI<sub>3</sub>, we used the lattice constants  $a = 8.995 \text{ \AA}$  and  $c = 12.685 \text{ \AA}$ , which are the equilibrium lattice constants at room temperature predicted using quasi-harmonic approximation.<sup>68,72</sup> The computed room temperature lattice constants  $a$  and  $c$  respectively overestimate by 1% and 0.1 % the experimental values measured on large crystalline samples<sup>73</sup>.

For to polaron computations, to optimize the geometry, we evaluate first the pSIC forces on top of Perdew-Burke-Ernzerhof (PBE)<sup>62</sup> with Tkatchenko-Scheffler van der Waals dispersion correction<sup>64</sup>. Then using the optimized structure the final pSIC energy is calculated by taking into account perturbative spin-orbit coupling (SOC)<sup>65</sup>. While SOC corrections are needed to correctly describe the electronic structure in MAPbI<sub>3</sub>, these also have appreciable effect for the energetics in MAPbI<sub>3</sub> as shown before.<sup>51,74</sup> The final energy is also calculated in the framework of pSIC taking into account SOC and vdW correction but using Heyd-Scuseria-Ernzerhof (HSE06)<sup>63</sup> DFT functional. The polaron structural optimization was carried out using  $2 \times 2 \times 1$   $\Gamma$ -centered k-point mesh for the  $2 \times 2 \times 2$  supercell ( $a = 17.99 \text{ \AA}$  and  $c = 25.37 \text{ \AA}$ ) with 384 atoms. The final polaron energies are reported using  $4 \times 4 \times 2$   $\Gamma$ -centered k-point mesh in the same supercell. We found the difference between the formation energies obtained with  $2 \times 2 \times 1$  and  $4 \times 4 \times 2$   $\Gamma$ -centered k-point meshes to be less than 0.02 eV. The optimization convergence cutoff is  $10^{-5} \text{ eV/\AA}$  for the maximum net force on atoms, while the while the self-consistent-field convergence criterion is based on total energy difference equal to  $10^{-5} \text{ eV}$ . The band structures were generated taking into account SOC. The band structures of hole and electron polarons were generated from the bands structures of charged systems (i.e., +1 for hole and -1 for electron polaron).

#### IV. RESULTS AND DISCUSSION

We have investigated the polaron states in tetragonal MAPbI<sub>3</sub> using a 2×2×2 supercell with 384 atoms. Band structure calculated with PBE, HSE06, and accurate *GW* calculations agree that the conduction band minimum (CBM) is composed mainly of 6*p*-orbitals of lead, while the valence band maximum (VBM) is composed of 6*s*-orbitals of lead and 5*p*-orbitals of iodine<sup>14,35,51,52</sup>. The self-trapping is expected to take place via the orbitals of CBM (VBM) in case of electron (hole) polaron, as already seen in previous studies without self-interaction correction<sup>75–82</sup>. Starting from the ground configuration of MAPbI<sub>3</sub>, we have optimized the polaron states using different initial configurations that vary by the amount of displacements of one of the Pb-I bonds associated with the polaron site. To assess if the methylammonium (MA) dipole moment has an effect on the polaron state, we have utilized initial guess structures with different orientations of dipole moment of MA. The MA dipole moments within a sphere of radius  $\sim 6$  Å, for an electron were preferentially oriented toward the polaron site, or away from it in case of hole. The model of MA dipole moment was done to evaluate its impact on the geometry of the structure, as its presence in MAPbI<sub>3</sub> is supported by optical-pump, terahertz-probe<sup>30</sup>. However, we have observed in our calculations that structures produced with different MA dipoles as initial guess have no effect on the final optimized polaron structures.

To evaluate the stability of small polaron, we have calculated the polaron binding energies, Eqs. (4) and (8), corrected for fictitious long-range interactions,  $E_{corr}^{el-st}(\Omega)$ , due to finite supercell volume,  $\Omega$ ,<sup>55</sup> see Tab. I.

TABLE I: Polaron formation energies and polaron levels in *eV* before and after correcting for fictitious long electrostatic interactions,  $E_{corr}^{el-st}(\Omega)$ . Values are obtained from pSIC on top of PBE+SOC(vdW-TS) and HSE+SOC(vdW-TS).

$h^+$	$\Delta E$	$\Delta\epsilon^{HOMO}$	$\Delta\epsilon_{corr}^{HOMO}$	$E_{bind}^+$	$E_{bind,corr}^+$
PBE	0.999	0.888	1.215	0.111	-0.052
HSE	1.459	0.993	1.320	0.466	0.302
$e^-$	$\Delta E$	$\Delta\epsilon^{LUMO}$	$\Delta\epsilon_{corr}^{LUMO}$	$E_{bind}^-$	$E_{bind,corr}^-$
PBE	1.447	-0.118	-0.444	1.329	1.166
HSE	1.444	-0.170	-0.497	1.274	1.110

$E_{corr}^{el-st}(\Omega)$  is a generalisation of Freysoldt *et al.* correction<sup>61</sup> that takes into account also the acoustic phonon deformation potential (ADP), which is described by the real part of dielectric constant at high frequency,  $\epsilon(\infty)$ , via a modification of the long-range interaction potential<sup>55</sup>:

$$E_{corr}^{el-st}(\Omega) = -\left(\frac{1}{\epsilon(\infty)} - \frac{1}{\epsilon(0)}\right) \frac{e^2}{r\epsilon_0}, \quad (13)$$

where  $r$  is the distance from the polaron site,  $e$  is the electron charge and  $\epsilon_0$  is the vacuum permittivity. For

MAPbI<sub>3</sub> at room temperature, the experimental values of  $\epsilon(\infty)$  and  $\epsilon(0)$  (the real part of dielectric constant at low frequency) are 5.4 and 60, respectively<sup>34</sup>, and the corresponding correction is  $-0.163$  *eV* for both hole and electron polarons (see Tab. I). Thus, we find that the correction very weakly depends on polaron radii, which are substantially different for the electron (3.24 Å) and hole (1.09 Å) cases. The correction for the polaron level with respect to band edge is twice the binding-energy correction in accordance with the Pekar's theorem<sup>83</sup>, and it is expressed in case of *HOMO* as<sup>55</sup> as follows:

$$\Delta\epsilon_{corr}^{HOMO} = \Delta\epsilon^{HOMO} + 2E_{corr}^{el-st}(\Omega), \quad (14)$$

and similarly for *LUMO* level. As seen from Tab. I,  $E_{bind,corr}^-$  calculated with both PBE+SOC(vdW-TS) and HSE+SOC(vdW-TS) agree with each other showing an unstable electron polaron with a positive binding energy that is much higher than thermal energy at normal conditions.  $E_{bind,corr}^+$  calculated with PBE+SOC(vdW-TS) and HSE+SOC(vdW-TS) are close to zero suggesting that the sign is ambiguous. The geometry was optimized with pSIC+PBE and subsequently the calculation of total energy and electronic structure was performed with the more accurate but computationally expensive HSE<sup>84–89</sup>. Thus, the hole binding energy obtained with HSE+SOC(vdW-TS) is overestimated by  $\sim 0.1$  *eV*<sup>84–89</sup>, so that our estimated value for the binding energy becomes 0.2 *eV*, a value whose uncertainty is estimated 0.1 *eV*, due to e.g. HSE inherent errors<sup>89</sup> or electron-phonon effects<sup>90</sup>. Moreover, the Coulomb interaction of localized holes with compensating electrons in photoexcited sample will further stabilize the self-trapped state. In addition, the excess photon energy above the gap can push the system close to the metastable state during thermalization. Thus, the small hole polaron is metastable and can be present at room temperature in photoexcited materials. Such 0.2 *eV* hole polaron formation energy must be provided by thermal fluctuations, which for room temperature operation mode delivers about one such small polaron over ten thousand generated holes. This explains the observed small increase of  $k_2$  around room temperature. At higher temperatures, the life-time of small hole polarons decreases, and the  $k_2$  temperature dependence is again consistent with large-polaron picture (i.e., monotonically decreases).

Looking in detail at structural rearrangements associated with the polaron, we can observe in Fig. 1 that the polaron stabilization is accompanied by considerable structural changes, including bond compression and dilatation, or even formation of a new bond of 3.5 Å between two iodine atoms in the case of the hole polaron. As seen in Fig. 1, the polaron disrupts the octahedral symmetry of the lattice near the localization site. For example, the electron localized at Pb disrupts the equivalent Pb-I bonds of  $\sim 3.2$  Å with the six neighboring iodine atoms. This breaking of octahedral symmetry induces an

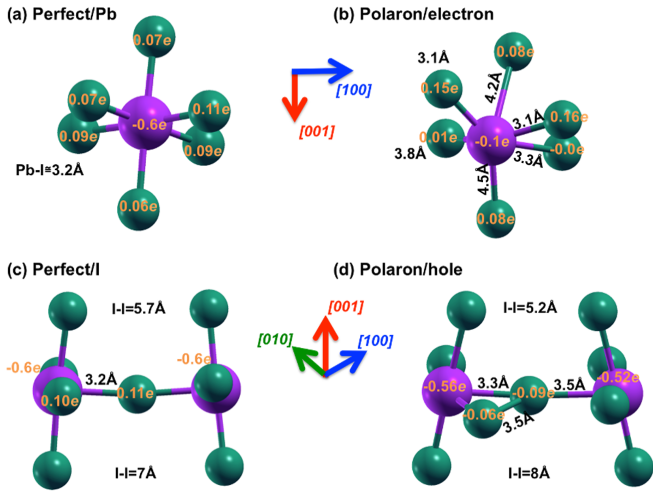


FIG. 1: Atomic structure of the (a, b) electron and (c, d) hole polarons near the localization site before (a, c) and after (b, d) optimization. Bond lengths and Löwdin charges are shown. Pb and I are represented as purple and green spheres, respectively.

axial elongation from 3.2 to 4.2-4.5 Å. While, the equatorial bonds have a slight variation by  $\sim 0.1$  Å. Our results are in line with those were obtained on MAPbI<sub>3</sub> with isolated cluster approach<sup>46–48</sup> where an axial variation is obtained from 3.3 to 4.2 Å and equatorial bonds have the the same our slight variation. We can also observe the global geometry change in Fig. 2a. Entering in details we see that the hole polaron generates a symmetry distortion with two Pb-I bond lengths increase from about 3.2 Å in the pristine system to 3.3 and 3.5 Å in the polaron structure and the formation of I<sub>2</sub><sup>-</sup> between two Pb elements, see Fig. 1d. The formation of I<sub>2</sub><sup>-</sup> molecule is observed also in previous works with isolated cluster approach<sup>46–48</sup>, but the I-I bond length was not reported in these previous studies.

Löwdin charge decomposition for the *neutral* system shows that Pb loses 0.6 electrons to iodine atoms in the perfect geometry. The distorted geometry for electron polaron, with an increase of several bond lengths allows for the electron localization in the Pb vicinity. The Löwdin analysis yields an increase of 0.5 electron on the Pb site. The natural bond orbital wavefunctions for both electron and hole are shown in Fig. 2a,b. The increase in the Pb-Pb distance from 6.4 Å in the perfect crystal to 6.81 Å for the hole polaron is expected considering the repulsive electrostatic interactions between Pb<sup>2+</sup> and the hole localized at iodine, or equivalently because the positive charge at iodine decreases the electrostatic attraction between Pb<sup>2+</sup> and I<sup>-</sup>. In the perovskite structure, each Pb<sup>2+</sup> is coordinated by 6 I<sup>-</sup>. The hole polaron formation is facilitated by removing one electron from one I<sup>-</sup> that changes the valence electronic configuration from  $4d^{10}5s^25p^6$  to  $4d^{10}5s^25p^5$ . To regain the necessary electron with respect the “octet rule”, this iodine atom forms a covalent bond with another I<sup>-</sup> by sharing an electron,

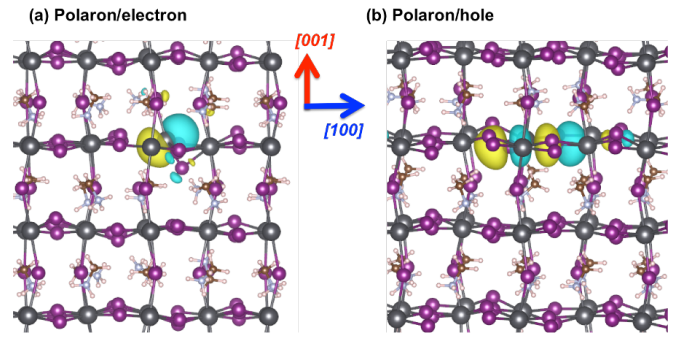


FIG. 2: Natural bond orbital wavefunctions calculated using HSE+SOC(vdW-TS) for (a) electron and (b) hole polaron states, at their pSIC optimized geometries. The isovalue surfaces of the wavefunctions correspond to a square modulus of the wavefunction equal to  $0.01 e/\text{Å}^3$ . Legend: yellow corresponds to the positive phase of wavefunction; cyan corresponds to negative phase of wavefunction.

thus forming I<sub>2</sub><sup>-</sup>. This charge rearrangement is also consistent with the structural changes resulting in a I-I bond distance equal to 3.5 Å, see Fig. 1d.

The formation of polaron does not only generate a geometrical distortion, but the polaron charge is localized on specific orbitals, which is indicative of the polaron size. One can determine on which orbitals the self-trapping is localized from the analysis of the orbital character of the polaron Kohn-Sham state within the gap, at the optimized pSIC geometry. The additional electron is situated on the  $6p$ -orbital of Pb, see Fig. 2a. Similarly, in case of hole there is a lattice distortion, mainly near the iodine atoms that create I<sub>2</sub><sup>-</sup> diatomic moiety, and the hole is trapped in antibonding  $\sigma$ -type orbital of this I<sub>2</sub><sup>-</sup>, composed of  $5p$ -orbitals, see Fig. 2b.

The localization of hole polaron on the halogen species<sup>91</sup> explains tolerance of charge-carrier mobility to halogen substitutions with isovalent atoms. As known from literature<sup>53,92,93</sup>, substituting I with Br improves the solar efficiency of MAPbI<sub>3</sub>-based solar cells. Br has a higher electronegativity ( $\chi$ ) than I (3.45 versus 3.2 according to Tantardini-Oganov scale<sup>94</sup>), and therefore a further destabilization of hole polaron is expected in the presence of Br, which is beneficial for solar cells. To investigate this further, we have carried out full pSIC calculations on doped supercells where we substituted one I with Br ( $\chi = 3.45$ ) or Cl ( $\chi = 3.5$ ). Our results show that doped MABPI<sub>3</sub> with either Br or Cl would destabilize the hole polaron by 0.06 eV and 0.12 eV, respectively. Thus, we have confirmed that the introduction of highly electronegative halogen decreases the already low probability of self-trapping in MAPbI<sub>3</sub>, which guarantees high  $L_D$  and non-Langevin behaviour that are required to have a good solar cell absorber.

We look now for the effects of self-trapping on the electronic band structure. Fig. 3 shows band structure of pristine MAPbI<sub>3</sub>. We can observe around the  $\Gamma$  point a linear split-off, which is a consequence of the Rashba-

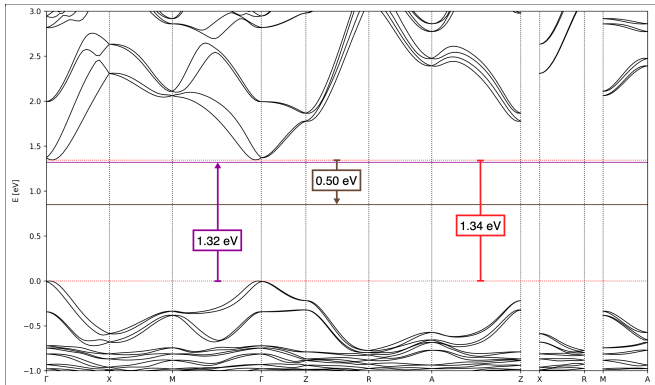


FIG. 3: Band structure of pristine MAPbI<sub>3</sub> with polaron levels (in eV) calculated using pSIC with HSE+SOC(vdw-TS) functional. The numbers show band gap of the pristine material (red), electron (brown), and hole (purple) polaron levels.

Dresselhaus splitting due to spin-orbit coupling<sup>95</sup>. The band gap is 1.34 eV, in reasonable agreement with the 1.5 eV band gap of Yin et al.<sup>96</sup> for the cubic geometry (while ours is a relaxed tetragonal geometry). Electron polaron level calculated using pSIC with HSE+SOC(vdw-TS) functional (and corrected for the supercell effects as described in Ref. 55) is 0.50 eV below the CBM (rounded from -0.497 eV in Tab. I). It is interesting that the hole polaron's level is shifted very close to CBM (0.02 eV below CBM), see Fig. 3). This is due to the hole localization at the high-energy  $\sigma$  antibonding orbital of the  $I_2^-$  moiety. Together with the predicted metastability of the hole, this implies that at finite temperature the barrier for  $I_2^-$  formation and hole localization can be overcome by at least a fraction of the holes, with the polaron level being remarkably close to CBM. These results explain the experimentally observed small Stokes shifts (of the order of meV) between absorption onset and photoluminescence emission peaks<sup>40,45</sup>. It is noteworthy that metastable hole polaron with level close to CBM can contribute to the non-Langevin behaviour<sup>14,17,20,30</sup>. Moreover, the presence of a shallow minimum on the potential-energy surface, corresponding to the metastable hole with compensating electron in the conduction band, can explain the enhanced anharmonicity in MAPbI<sub>3</sub><sup>30,97,98</sup>.

## V. CONCLUSION

In this work we have performed first-principles calculations of electron and hole polarons in tetragonal MAPbI<sub>3</sub> phase using an advanced approach that combines hybrid

DFT calculations, SOC corrections, long range van der Waals and electrostatic interactions, and pSIC to investigate self-trapping of charge carriers in MAPbI<sub>3</sub>. We show that our results explain recent experimental details owing to the absence of SIE in our computational framework. The application of this state-of-the-art approach allowed us to resolve discrepancies between previous theoretical and experimental studies. Our calculations showed that the creation of a small electron polaron is always unstable in MAPbI<sub>3</sub>. On the other hand, a small hole polaron state is metastable, but likely thermally accessible due to the proximity of the small hole polaron energy to CBM. Actually, hole polaron is localized on the high-energy  $\sigma$  antibonding orbital of the  $I_2^-$  moiety. This along with the existence of large polarons explains the non-monotonic behaviour of  $k_2$  at room-temperature. Furthermore, we showed that doping with anion-substituting impurities such as Br and Cl results in further destabilization of small polarons, which explains why Br and Cl impurities are non-detrimental to hole mobility. The underpinnings of the benign effects of these substitutions on the polaron stability is due to the higher electronegativity of Br and Cl compared to I, which increases the localization energy for the hole. Based on this work and previous studies, we posit that the difference of one order of magnitude between ionic displacements (i.e., ~MHz) and molecular vibrations (i.e., ~GHz) leads to a delocalized polaron over several MAPbI<sub>3</sub> units cells and inhibits the stability of self-trapping.

## Acknowledgments

W.A.S. acknowledges the financial support from the National Science Foundation Award Nos. DMR-1809085 and CSSI-2003808. S.V.L. acknowledges support by RSCF-INSF grant 20-53-56065. X.G. acknowledges funding from the FRS-FNRS Belgium under grant number T.0103.19 - ALPS. C.T. acknowledges the Russian state assignment to ISSCM SB RAS (project No 1021051402751-7-1.4.3). Calculations were performed in part at the Argonne Leadership Computing Facility, which is a DOE Office of Science User Facility supported under Contract DE-AC02-06CH11357, Extreme Science and Engineering Discovery Environment (XSEDE), the University of Pittsburgh Center for Research Computing (CRC) through the computational resources provide, and Siberian Super-Computer Center of the Siberian Branch of the Russian Academy of Sciences for computational resources.

<sup>1</sup> L. R. V. Buizza and L. M. Herz, *Advanced Materials* **33**, 2007057 (2021).

<sup>2</sup> M. A. Green, A. Ho-Baillie, and H. J. Snaith, *Nature*

*Photonics* **8**, 506 (2014).

<sup>3</sup> H. S. Jung and N.-G. Park, *Small* **11**, 10 (2014).

<sup>4</sup> B. Wang, X. Xiao, and T. Chen, *Nanoscale* **6**, 12287

- (2014).
- <sup>5</sup> H. J. Snaith, *The Journal of Physical Chemistry Letters* **4**, 3623 (2013).
  - <sup>6</sup> P. Gao, M. Grätzel, and M. K. Nazeeruddin, *Energy Environ. Sci.* **7**, 2448 (2014).
  - <sup>7</sup> S. Brittman, G. W. P. Adhyaksa, and E. C. Garnett, *MRS Communications* **5**, 7 (2015).
  - <sup>8</sup> A. Kojima and et al., *J. Am. Chem. Soc.* **131** (17), 6050 (2009).
  - <sup>9</sup> H.-S. Kim, C.-R. Lee, J.-H. Im, K.-B. Lee, T. Moehl, A. Marchioro, S.-J. Moon, R. Humphry-Baker, J.-H. Yum, J. E. Moser, M. Grätzel, and N.-G. Park, *Scientific Reports* **2**, 591 (2012).
  - <sup>10</sup> M. M. Lee, J. Teuscher, T. Miyasaka, T. N. Murakami, and H. J. Snaith, *Science* **338**, 643 (2012).
  - <sup>11</sup> J. S. Manser, J. A. Christians, and P. V. Kamat, *Chemical Reviews* **116**, 12956 (2016).
  - <sup>12</sup> L. M. Herz, *Annual Review of Physical Chemistry* **67**, 65 (2016).
  - <sup>13</sup> T. M. Brenner, D. A. Egger, L. Kronik, G. Hodes, and D. Cahen, *Nature Reviews Materials* **1**, 15007 (2016).
  - <sup>14</sup> C. Wehrenfennig and et al., *The Journal of Physical Chemistry Letters* **5**(8), 1300 (2014).
  - <sup>15</sup> L. M. Herz, *ACS Energy Letters* **2**, 1539 (2017).
  - <sup>16</sup> L. Protesescu, S. Yakunin, M. I. Bodnarchuk, F. Krieg, R. Caputo, C. H. Hendon, R. X. Yang, A. Walsh, and M. V. Kovalenko, *Nano Letters* **15**, 3692 (2015).
  - <sup>17</sup> M. B. Johnston and L. M. Herz, *Accounts of Chemical Research* **49**, 146 (2016).
  - <sup>18</sup> F. Giustino, *Rev. Mod. Phys.* **89**, 015003 (2017).
  - <sup>19</sup> J. Frost, K. T. Butler, and A. Walsh, *APL Materials* **2** (8), 081506 (2014).
  - <sup>20</sup> J. M. Frost, *Phys. Rev. B* **96**, 195202 (2017).
  - <sup>21</sup> M. Sendner, P. K. Nayak, D. A. Egger, S. Beck, C. Müller, B. Epding, W. Kowalsky, L. Kronik, H. J. Snaith, A. Pucci, and R. Lovrinčić, *Mater. Horiz.* **3**, 613 (2016).
  - <sup>22</sup> M. Schlipf, S. Poncé, and F. Giustino, *Phys. Rev. Lett.* **121**, 086402 (2018).
  - <sup>23</sup> S. Poncé, M. Schlipf, and F. Giustino, *ACS Energy Letters* **4**, 456 (2019).
  - <sup>24</sup> S. J. Zelewski, J. M. Urban, A. Surrente, D. K. Maude, A. Kuc, L. Schade, R. D. Johnson, M. Dollmann, P. K. Nayak, H. J. Snaith, P. Radaelli, R. Kudrawiec, R. J. Nicholas, P. Plochocka, and M. Baranowski, *J. Mater. Chem. C* **7**, 8350 (2019).
  - <sup>25</sup> T. Holstein, *Annals of Physics* **8**, 343 (1959).
  - <sup>26</sup> G. Hodes and P. V. Kamat, *The Journal of Physical Chemistry Letters* **6**, 4090 (2015).
  - <sup>27</sup> T. Brenner and et al., *The Journal of Physical Chemistry Letters* **6**, 4754 (2015).
  - <sup>28</sup> R. Gottesman, L. Gouda, B. S. Kalanoor, E. Haltzi, S. Tirosh, E. Rosh-Hodesh, Y. Tischler, A. Zaban, C. Quarti, E. Mosconi, and F. De Angelis, *The Journal of Physical Chemistry Letters* **6**, 2332 (2015).
  - <sup>29</sup> H. Oga, A. Saeki, Y. Ogomi, S. Hayase, and S. Seki, *Journal of the American Chemical Society* **136**, 13818 (2014).
  - <sup>30</sup> L. M. Herz, *The Journal of Physical Chemistry Letters* **9**, 6853 (2018).
  - <sup>31</sup> R. L. Milot, G. E. Eperon, H. J. Snaith, M. B. Johnston, and L. M. Herz, *Advanced Functional Materials* **25**, 6218 (2015).
  - <sup>32</sup> T. J. Savenije, C. S. Ponseca, L. Kunneman, M. Abdellah, K. Zheng, Y. Tian, Q. Zhu, S. E. Canton, I. G. Scheblykin, T. Pullerits, A. Yartsev, and V. Sundström, *The Journal of Physical Chemistry Letters* **5**, 2189 (2014).
  - <sup>33</sup> M. Karakus, S. A. Jensen, F. D'Angelo, D. Turchinovich, M. Bonn, and E. Cánovas, *The Journal of Physical Chemistry Letters* **6**, 4991 (2015).
  - <sup>34</sup> S. Shrestha, G. J. Matt, A. Osvet, D. Niesner, R. Hock, and C. J. Brabec, *The Journal of Physical Chemistry C* **122**, 5935 (2018).
  - <sup>35</sup> D. Zhao, J. M. Skelton, H. Hu, C. La-o vorakiat, J.-X. Zhu, R. A. Marcus, M.-E. Michel-Beyerle, Y. M. Lam, A. Walsh, and E. E. M. Chia, *Applied Physics Letters* **111**, 201903 (2017).
  - <sup>36</sup> Y. Lan, B. J. Dringoli, D. A. Valverde-Chávez, C. S. Ponseca, M. Sutton, Y. He, M. G. Kanatzidis, and D. G. Cooke, *Science Advances* **5** (2019).
  - <sup>37</sup> S. Neutzner, F. Thouin, D. Cortecchia, A. Petrozza, C. Silva, and A. R. Srimath Kandada, *Phys. Rev. Materials* **2**, 064605 (2018).
  - <sup>38</sup> G. Batignani, G. Fumero, A. R. Srimath Kandada, G. Cerullo, M. Gandini, C. Ferrante, A. Petrozza, and T. Scopigno, *Nature Communications* **9**, 1971 (2018).
  - <sup>39</sup> J. M. Richter, M. Abdi-Jalebi, A. Sadhanala, M. Tabachnyk, J. P. Rivett, L. M. Pazos-Outón, K. C. Gödel, M. Price, F. Deschler, and R. H. Friend, *Nature Communications* **7**, 13941 (2016).
  - <sup>40</sup> W. Rehman, R. L. Milot, G. E. Eperon, C. Wehrenfennig, J. L. Boland, H. J. Snaith, M. B. Johnston, and L. M. Herz, *Advanced Materials* **27**, 7938 (2015).
  - <sup>41</sup> C. L. Davies, M. R. Filip, J. B. Patel, T. W. Crothers, C. Verdi, A. D. Wright, R. L. Milot, F. Giustino, M. B. Johnston, and L. M. Herz, *Nature Communications* **9**, 293 (2018).
  - <sup>42</sup> A. Beattie and P. Landsberg, *Proceedings of the Royal Society of London. Series A. Mathematical and Physical Sciences* **249**, 16 (1959).
  - <sup>43</sup> A. Haug, *Journal of Physics C: Solid State Physics* **16**, 4159 (1983).
  - <sup>44</sup> Y. He and G. Galli, *Chemistry of Materials* **26**, 5394 (2014).
  - <sup>45</sup> Y. Guo, O. Yaffe, T. D. Hull, J. S. Owen, D. R. Reichman, and L. E. Brus, *Nature Communications* **10**, 1175 (2019).
  - <sup>46</sup> D. Ghosh, E. Welch, A. J. Neukirch, A. Zakhidov, and S. Tretiak, *The Journal of Physical Chemistry Letters* **11**, 3271 (2020).
  - <sup>47</sup> A. J. Neukirch, W. Nie, J.-C. Blancon, K. Appavoo, H. Tsai, M. Y. Sfeir, C. Katan, L. Pedesseau, J. Even, J. J. Crochet, G. Gupta, A. D. Mohite, and S. Tretiak, *Nano Letters* **16**, 3809 (2016).
  - <sup>48</sup> W. Nie, J.-C. Blancon, A. J. Neukirch, K. Appavoo, H. Tsai, M. Chhowalla, M. A. Alam, M. Y. Sfeir, C. Katan, J. Even, S. Tretiak, J. J. Crochet, G. Gupta, and A. D. Mohite, *Nature Communications* **7**, 11574 (2016).
  - <sup>49</sup> Y. Wang, Y. Zhang, P. Zhang, and W. Zhang, *Phys. Chem. Chem. Phys.* **17**, 11516 (2015).
  - <sup>50</sup> W. H. Sio, C. Verdi, S. Poncé, and F. Giustino, *Phys. Rev. B* **99**, 235139 (2019).
  - <sup>51</sup> P. Umari, E. Mosconi, and D. A. F., *CrystEngComm* **4**, 4467 (2014).
  - <sup>52</sup> A. D. Wright and et al., *Nature Communication* **7**, 11755 (2016).
  - <sup>53</sup> A. E. Maughan, A. M. Ganose, A. M. Candia, J. T. Granger, D. O. Scanlon, and J. R. Neilson, *Chemistry of Materials* **30**, 472 (2018).
  - <sup>54</sup> Z. Xiao, W. Meng, J. Wang, D. B. Mitzi, and Y. Yan, *Mater. Horiz.* **4**, 206 (2017).

- <sup>55</sup> S. Kokott, S. V. Levchenko, P. Rinke, and M. Scheffler, *New Journal of Physics* **20**, 033023 (2018).
- <sup>56</sup> C. Spreako and J. VandeVondele, *Phys. Chem. Chem. Phys.* **16**, 26144 (2014).
- <sup>57</sup> B. Sadigh, P. Erhart, and D. D. Aberg, *Physical Review B* **92** (7), 075202 (2015).
- <sup>58</sup> B. Sadigh, P. Erhart, and D. D. Aberg, *Physical Review B* **92**, 199905(E) (2015).
- <sup>59</sup> G. Geneste, B. Amadon, M. Torrent, and G. Dezanneau, *Phys. Rev. B* **96**, 134123 (2017).
- <sup>60</sup> G. Makov and M. C. Payne, *Physical Review B* **51**, 4014 (1995).
- <sup>61</sup> C. Freysoldt, J. Neugebauer, and C. G. Van de Walle, *physica status solidi (b)* **248** (5), 1067 (2011).
- <sup>62</sup> J. Perdew, K. Burke, and M. Ernzerhof, *Physical Review Letters* **77**, 3865 (1996).
- <sup>63</sup> J. Heyd and G. E. Scuseria, *The Journal of Chemical Physics* **121**, 1187 (2004).
- <sup>64</sup> A. Tkatchenko and M. Scheffler, *Physical Review Letters* **102** (7), 073005 (2009).
- <sup>65</sup> W. P. Huhn and V. Blum, *Phys. Rev. Materials* **1**, 033803 (2017).
- <sup>66</sup> J. Feng and B. Xiao, *The Journal of Physical Chemistry Letters* **5** (7), 1278 (2014).
- <sup>67</sup> D. Egger and L. Kronik, *The Journal of Physical Chemistry Letters* **5** (15), 2728 (2014).
- <sup>68</sup> W. A. Saidi and J. J. Choi, *The Journal of Chemical Physics* **145**, 144702 (2016).
- <sup>69</sup> J. F. Janak, *Phys. Rev. B* **18**, 7165 (1978).
- <sup>70</sup> F. Gygi and A. Baldereschi, *Physical Review Letters* **62** (18), 2160 (1989).
- <sup>71</sup> B. Sadigh and et al., *Physical Review Letters* **106** (2), 027401 (2011).
- <sup>72</sup> W. A. Saidi and A. Kachmar, *The Journal of Physical Chemistry Letters* **9** (24), 7090 (2018).
- <sup>73</sup> Y. Dang and et al., *CrystEngComm* **17** (3), 665 (2015).
- <sup>74</sup> W. Shan and W. A. Saidi, *The Journal of Physical Chemistry Letters* **8** (23), 5935–5942 (2017).
- <sup>75</sup> Y. Toyozawa, *Progress of Theoretical Physics* **26**, 29 (1961).
- <sup>76</sup> Y. Toyozawa, *Journal of the Physical Society of Japan* **44**, 482 (1978).
- <sup>77</sup> A. M. Stoneham, J. Gavartin, A. L. Shluger, A. V. Kimmel, D. M. Ramo, H. M. Rönnow, G. Aeppli, and C. Renner, *Journal of Physics: Condensed Matter* **19**, 255208 (2007).
- <sup>78</sup> V. V. Kabanov and O. Y. Mashtakov, *Phys. Rev. B* **47**, 6060 (1993).
- <sup>79</sup> N. F. Mott and A. M. Stoneham, *Journal of Physics C: Solid State Physics* **10**, 3391 (1977).
- <sup>80</sup> Y. Unuma, Y. Masumoto, S. Shionoya, and H. Nishimura, *Journal of the Physical Society of Japan* **52**, 4277 (1983).
- <sup>81</sup> F. X. Morrissey, J. G. Mance, A. D. V. Pelt, and S. L. Dexheimer, *Journal of Physics: Condensed Matter* **25**, 144204 (2013).
- <sup>82</sup> S. Tomimoto, H. Nausei, S. Saito, T. Suemoto, J. Takeda, and S. Kurita, *Phys. Rev. Lett.* **81**, 417 (1998).
- <sup>83</sup> L. Lemmens and J. Devreese, *Solid State Communications* **12**, 1067 (1973).
- <sup>84</sup> S. J. Clark, J. Robertson, S. Lany, and A. Zunger, *Phys. Rev. B* **81**, 115311 (2010).
- <sup>85</sup> H. Xiao, J. Tahir-Kheli, and W. A. Goddard, *The Journal of Physical Chemistry Letters* **2**, 212 (2011).
- <sup>86</sup> J. P. Perdew, W. Yang, K. Burke, Z. Yang, E. K. U. Gross, M. Scheffler, G. E. Scuseria, T. M. Henderson, I. Y. Zhang, A. Ruzsinszky, H. Peng, J. Sun, E. Trushin, and A. Görling, *Proceedings of the National Academy of Sciences* **114**, 2801 (2017).
- <sup>87</sup> A. J. Garza and G. E. Scuseria, *The Journal of Physical Chemistry Letters* **7**, 4165 (2016).
- <sup>88</sup> P. Borlido, J. Schmidt, A. W. Huran, F. Tran, M. A. L. Marques, and S. Botti, *npj Computational Materials* **6**, 96 (2020).
- <sup>89</sup> P. Borlido, T. Aull, A. W. Huran, F. Tran, M. A. L. Marques, and S. Botti, *Journal of Chemical Theory and Computation* **15**, 5069 (2019).
- <sup>90</sup> A. Miglio, V. Brousseau-Couture, E. Godbout, G. Antonius, Y.-H. Chan, S. G. Louie, M. Côté, M. Giantomassi, and X. Gonze, *npj Computational Materials* **6**, 167 (2020).
- <sup>91</sup> C. Tantardini and E. Benassi, *Dalton Trans.* **47**, 5483 (2018).
- <sup>92</sup> B. Zhang, Y. Liao, L. Tong, Y. Yang, and X. Wang, *Phys. Chem. Chem. Phys.* **22**, 7778 (2020).
- <sup>93</sup> S. V. N. Pammi, V.-D. Tran, R. Maddaka, J.-H. Eom, J. S. Jung, H.-M. Jeong, M.-D. Kim, V. Pecunia, and S. G. Yoon, *Advanced Optical Materials* **8**, 2000845 (2020).
- <sup>94</sup> C. Tantardini and A. R. Oganov, *Nature Communications* **12**, 2087 (2021).
- <sup>95</sup> Z.-G. Yu, *The Journal of Physical Chemistry Letters* **7**, 3078 (2016).
- <sup>96</sup> W.-J. Yin, T. Shi, and Y. Yan, *Applied Physics Letters* **104**, 063903 (2014).
- <sup>97</sup> T. Debnath, D. Sarker, H. Huang, Z.-K. Han, A. Dey, L. Polavarapu, S. V. Levchenko, and J. Feldmann, *Nature Communications* **12**, 2629 (2021).
- <sup>98</sup> C. Gehrman and D. A. Egger, *Nature Communications* **10**, 3141 (2019).